Cellulose (2017) 24:1803–1814
DOI 10.1007/s10570-017-1210-4

ORIGINAL PAPER

Improvement of bagasse fiber–cement composites by addition of bacterial nanocellulose: an inverse gas chromatography study

F. Mohammadkazemi · R. Aguiar · N. Cordeiro

Received: 19 October 2016 / Accepted: 27 January 2017 / Published online: 9 February 2017

Abstract The design of green fiber-reinforced nanocomposites with enhanced properties and durability has attracted attention from scientists. The present study aims to investigate the potential of bacterial nanocellulose (BNC) as a green additive for fiber–cement composites. Inverse gas chromatography (IGC) was used to evaluate the influence of incorporation of BNC as powder or gel, or coated onto the bagasse fibers, on the fiber–cement composite (FCC) surface. The results indicated that BNC incorporation made the FCC surface more reactive, increasing the dispersive component of the surface energy. The most relevant effects were found for BNC incorporation as gel or coated on the fibers. Incorporation of BNC as gel resulted in a predominantly organic FCC surface with substantial decreased surface basicity (K_a/K_b ratio from 2.88 to 5.75). IGC also showed that FCC with BNC incorporated as gel was more susceptible to hydration. However, BNC coated on fibers prevented fiber mineralization, increasing the inorganic materials at the surface, which caused an increase in the surface basicity (K_a/K_b ratio decrease to 2.00). These promising results could contribute to development of a new generation of green hybrid composites. The IGC technique enabled understanding of the physicochemical changes that occur on deliberate introduction of nanosized bacterial cellulose into fiber–cement composites.

Keywords Bacterial nanocellulose · Bagasse fiber · Green composites · Inverse gas chromatography (IGC) · Fiber–cement composites

F. Mohammadkazemi (✉)
Department of Biosystems, Faculty of New Technologies Engineering, Shahid Beheshti University, Science and Research Campus, Zirab, Savadkooh, Mazandaran, Iran
e-mail: f_mkazemi@sbu.ac.ir

R. Aguiar · N. Cordeiro
Faculty of Science and Engineering, University of Madeira, Funchal, Portugal
e-mail: jrobertocaguiar@gmail.com

N. Cordeiro
e-mail: ncordeiro@uma.pt

Introduction

Due to growing environmental awareness and societal concern, together with the unsustainable consumption of petroleum and new environmental regulations, this century has witnessed remarkable achievements in green materials science technology. Increasing attention has been focused on natural fiber or green composites, including cellulosic fiber-reinforced composites. Cellulosic fibers provide adequate bonding capacity to cement-based matrices for substantial enhancement of their flexural strength, toughness, and impact resistance (Morton et al. 2010; Savastano et al. 2003). Furthermore, these fibers decrease the free plastic shrinkage (Tolêdo Filho et al. 2003),

decrease the thermal conductivity, and improve the acoustic performance by increasing sound absorption (Neithalath et al. 2004). Due to these advantages, fiber–cement composites (FCCs) have found practical commercial applications as replacements for hazardous asbestos materials. Today, FCC products can be widely found in siding and roofing materials and backer boards, among others.

Biofiber–cement composites are widely used in a large number of building and agricultural applications due to their versatility. The main reason for incorporating fibers as a reinforcing agent into a cement matrix is to produce a composite with improved toughness, ductility, flexural capacity, and crack resistance. One of the drawbacks associated with FCCs produced using ordinary Portland cement matrix is their limited durability, associated with the sensitivity of cellulose fibers to water, carbonation, and strong alkalis, and the generation of incompatible stresses (Fan et al. 1999, 2004). Loss of adhesion at the fiber–cement interface and increasing micro- and macrocracks contribute to strength and durability losses of such fiber–cement composites (John et al. 1998).

In recent studies, nanoscale cellulose was highlighted as an interesting green reinforcement agent for production of nanocomposites. Nanocellulose can be extracted from plants, but the required pulping and bleaching processes are not environmentally friendly. Bacterial nanocellulose (BNC), on the other hand, has great potential as a biological reinforcement for use in nanocomposites, due to its uniform dispersion, thermal stability, moisture absorption, and compatibility with common matrices used in composites. Recent research started to investigate the potential use of BNC in FCCs containing bagasse pulp fibers and the effect on fiber–cement interfaces (Mohammadkazemi et al. 2015). An important aspect to be determined for manufacture of new materials is their surface properties. Surprisingly, few studies are available in literature on the surface properties and wettability of cementitious materials (Benzarti et al. 2006; Cook and Hover 1993; Courard 1999; Grattoni et al. 1995; Momber 2002; Philippi and Souza 1995).

Inverse gas chromatography (IGC) is a useful and fairly versatile technique for characterization of the surface of composites, providing information on the physicochemical properties over wide temperature and humidity ranges. The flexibility of the IGC technique makes it a valuable tool for characterization of various materials, overcoming problems typically found with methods based on contact angle measurements, such as surface roughness, porosity, etc. For this reason, IGC has been successfully applied in batch-to-batch studies involving synthetic or biological materials, adsorbents (Elizalde-González and Ruíz Palma 1999), foods (Boutboul et al. 2002), carbon blacks (Papirer et al. 1999), nanocomposites (Boukerma et al. 2006), fillers (Milczewska and Voelkel 2002), and fibers (Castro et al. 2015; Cordeiro et al. 2011a, b). Characterization of hardened cement pastes by IGC was also reported in a few papers (Baeta Neves et al. 2002, 2004; Oliva et al. 2002).

The aim of the present work is to study in detail the effect of incorporation of bacterial nanocellulose on the surface of fiber–cement composites using IGC at infinite dilution.

Materials and methods

Materials

Unbleached bagasse pulp fibers were provided by a papermaking factory in Khuzestan, Iran. The average length, diameter, and lignin content of the fibers were 1.13 mm, 29.5 μm, and 2.7 wt%, respectively. Type II Portland cement was used, having specific surface area of 2600 $cm^2\ g^{-1}$ and specific gravity of 3–3.25 ton m^{-3}. Calcium chloride (Sigma-Aldrich) and polycarboxylate-based superplasticizer (Fabir Company, light-brown liquid with specific gravity of 1.05 g cm^{-3}) were used.

To produce bacterial nanocellulose (BNC), the bacterial strain *Gluconacetobacter xylinus* was cultured in Hestrin–Schramm medium as described in Mohammadkazemi et al. (2015).

BNC was prepared in three forms: powder, gel, and coated onto bagasse fibers. To prepare BNC powder (denoted by P), BNC was freeze-dried using a freeze-drier (SCANVAC, cool safe) at −92 °C and 0.02 hPa for 2 days. The particle size, measured using a Zetasizer ZEN 3600 by dynamic light scattering, was less than 75 nm. For preparation of gel (denoted by G), BNC was blended using a blender to produce a uniform dispersion. The crystallinity of the BNC was 65% as measured by X-ray diffraction (XRD) analysis. The particle size of the BNC gel was the same as

that of the BNC powder. To obtain BNC coated on bagasse fibers (denoted by C), a dispersion of 0.1 wt% BNC was prepared in deionized water, to which bagasse fibers were added and left at 30 °C overnight. Thereafter, coated fibers were vacuum filtered to remove additional water.

IGC measurements were carried out on samples using several probe molecules of GC grade (>99% purity) supplied by Sigma–Aldrich. Methane (>99.99% purity) was used as noninteracting reference probe, and the carrier gas was helium (>99.99% purity) supplied by Air Liquide Company.

Production of fiber–cement composites (FCCs)

Based on preliminary testing of FCCs, an optimum dry weight fraction of 6 wt% in bagasse fibers was chosen (Mohammadkazemi et al. 2015). The amount of BNC was the same for all the FCCs, i.e., 50 wt% relative to dry weight of bagasse fibers, but the type of BNC was different (P, C, or G). The fiber–cement composites were named P FCC, C FCC, and G FCC, respectively. The samples were also compared with fiber–cement composite without BNC (denoted as FCC only).

To produce the FCCs, we used polycarboxylate superplasticizer (0.5 wt% dry weight of cement) as water reducer and $CaCl_2$ (5 wt% to dry weight of cement) as catalyst, both dissolved in water and added to cement, fibers, and BNC. This mortar was mixed using an electric mixer for 5 min (3 min mixing with two 1-min pauses). The mixture was uniformly poured and distributed on a metal plate inside a frame-like mold, then another plate was placed on top of the mat. Thereafter, the mat was pressed until it reached the required thickness after 24 h of curing time. The composite was released from the mold and conditioned at 95% relative humidity (RH) and 20 ± 1 °C for 28 days. These cured FCCs were then conditioned and dried at 65 ± 2% RH and 20 ± 1 °C for 1 month.

Water absorption (WA)

To measure the water absorption according to DIN 68763 standard, eight samples with dimensions of 25 × 25 × 12 mm^3 from each treatment were cut and immersed in water for 2 h. The water absorption was calculated as a percentage of the initial sample weight before immersion in water.

Fourier-transform infrared (FTIR) spectrometry

Before analysis, the samples were dried to remove moisture. FTIR spectra were recorded using a PerkinElmer spectrophotometer in the range from 4000 to 400 cm^{-1} with resolution of 8 cm^{-1} and accumulation over 36 scans.

Inverse gas chromatography (IGC)

IGC measurements were carried out on a commercial inverse gas chromatograph (*i*GC, Surface Measurements Systems, London, UK) equipped with flame ionization detector (FID) and thermal conductivity detector (TCD). The *i*GC system is fully automatic, using the SMS *i*GC Controller v1.8 control software. Standard silanized (dimethyldichlorosilane; Repelcote BDH, UK) glass columns with 0.2 cm internal diameter (ID) and 30 cm length were used.

Columns containing the samples were placed in the IGC column oven module and conditioned overnight using helium at flow rate of 10 ml/min to remove impurities adsorbed on the surface. After conditioning at the measurement conditions, pulse injections were carried out with a 0.25-ml gas loop. The retention time was calculated from the FID response using the dead time of the tracer (methane) molecule. The retention volume and subsequent data were analyzed using *i*GC Standard v1.3 and Advanced Analysis Software v1.25.

Measurements of the dispersive surface interaction were performed using high-purity-grade *n*-alkanes (hexane, heptane, octane, nonane, and decane) at three temperatures (25, 27, and 29 °C) with carrier gas (helium) flow rate of 10 ml/min. Due to the higher surface energy of the G FCC sample, the measurement had to be carried out at 45, 50, and 55 °C. The oven temperature was controlled within ±0.1 °C. The *i*GC equipment is completely automated and can control the relative humidity (RH) of the samples from 0 to 90%. In this work, the dispersive surface interactions were investigated at 0 and 10% RH.

Acetonitrile (AcN), ethyl acetate (EtOAc), ethanol (EtOH), acetone (AC), and tetrahydrofuran (THF) were used to determine the Gibbs specific free energy (ΔG_S^{SP}) and acid–base surface character (K_a and K_b) at 25 or 50 °C (G FCC sample) and 0% RH.

To determine the Brunauer–Emmett–Teller (BET) surface area (S_{BET}) and monolayer capacity (n_m), isotherms were determined experimentally using *n*-

octane at p/p_0 values of 0.05, 0.07, 0.09, 0.1, 0.2, 0.4, 0.6, 0.8, and 0.95 at 25 or 50 °C (G FCC sample) and 0% RH with flow rate of 10 ml/min.

Permeability studies (to determine the energetic profile and adsorption potential, A_{max}) were performed using *n*-octane at p/p_0 of 0.2 with flow rate of 7, 10, 13, 16, 19, 22, 25, 28, 31, and 34 ml/min, at 25 or 50 °C (G FCC sample) and 0% RH.

The experiments were performed in duplicate, with results presented as average values. The experimental error due to variations in temperature, flow rate, and retention time measurements was estimated to be below 4%. The measurements and theory applied herein were described exhaustively by the authors in previous papers (Cordeiro et al. 2011a, b).

Scanning electron microscopy (SEM) and energy-dispersive X-ray spectroscopy (EDX)

Scanning electron microscopy (SEM, Philips XL 30), equipped with secondary-electron (SE) and backscattered-electron (BE) detectors, at voltage of 20 kV was used for microstructural analysis of fracture surfaces and characterization of fiber–cement interfaces in FCCs. Prior to field-emission (FE)-SEM and SEM observations, all samples were dried and gold coated. In addition, determination of the chemical composition of the samples and semiquantitative analysis of the surface and inside the fiber lumens were carried out using energy-dispersive X-ray spectroscopy (EDX).

X-ray diffraction (XRD) analysis

XRD analysis at 40 kV and 30 mA in the 2θ range of 4–60° was used for phase identification of the samples. Before XRD measurements, the samples were ground using a planetary ball mill (Fritsch, Pulverisette 5) to below 75 μm.

Results and discussion

The dispersive and acid–base properties of the surface affect the physicochemical interactions and tridimensional stability of cement composites. However, despite their importance, few studies have been published on these aspects, due to the complex composition of cementitious materials, with several different mineral phases, multiscale porous structure, and complex acid–base behavior.

In was intended to carry out all tests in this study at 25 °C, close to ambient temperature. However, it was observed experimentally that G FCC presented high retention time for the probes at this temperature. Therefore, temperatures of 45, 50, and 55 °C were used to determine the parameters for this sample.

Surface energy

The dispersive surface energy (γ_S^D) was determined using a series of *n*-alkanes from hexane to decane. All samples showed good correlation coefficients (0.990–0.999). Two sets of temperatures were used to study the behavior of γ_S^D versus temperature: (1) a lower range of 25, 27, and 29 °C, and (2) a higher range of 45, 50, and 55 °C (Table 1). A decrease of γ_S^D with increase of temperature is visible, which can be explained by the thermodynamics of the adsorption process, which is an exothermic phenomenon, so increasing the temperature makes adsorption less favorable (Keller and Staudt 2005). Linear decrease of γ_S^D with increase of temperature is observed (Table 1), which is frequent in cellulosic-based materials (Cordeiro et al. 2011a, b, 2012). Due to this linear dependence, it was possible to extrapolate and determine the magnitude of the γ_S^D value at 25 °C for the sample (G FCC) studied at higher temperature from the plot of γ_S^D versus temperature.

Bagasse fibers and BNC presented γ_S^D values (Table 1) close to those reported in literature (Cordeiro et al. 2011a, b; Gulati and Sain 2006; Mohammadkazemi et al. 2016). Portland cement presented a γ_S^D value of 42.97 mJ m^{-2} at 25 °C, within the range found in previous works; Baeta Neves et al. (2004) and Benzarti et al. (2006) studied different samples of ordinary Portland cement and determined values between 40 and 45 mJ m^{-2} (at 35 °C). In a more recent work, Carmona-Quiroga et al. (2011) determined the surface energy of various construction materials, obtaining 48.87 mJ m^{-2} at 50 °C for cement paste. The FCCs presented higher values of γ_S^D compared with the raw materials (bagasse fibers, BNC, and cement), showing that the FCC production process significantly changed the cement surface.

Variation in γ_S^D may be due to the type, number, and/or energy of active sites, which can be studied

Table 1 Dispersive component of surface energy (γ_S^D) and its variation with temperature ($\Delta\gamma_S^D/\Delta T$) for raw materials and bagasse fiber–cement composites

Sample	γ_S^D (mJ m^{-2})[a]			$(\Delta\gamma_S^D/\Delta T)$ (mJ m^{-2} K^{-1})
	25 °C	27 °C	29 °C	
Bagasse fiber	44.43	44.26	43.64	0.20
Bacterial nanocellulose	39.21	38.60	37.98	0.31
Portland cement	42.97	42.58	40.05	0.44
FCC	78.15	77.37	76.40	0.11
P FCC	86.05	83.92	80.80	1.31
C FCC	115.45	109.52	104.95	2.63
	45 °C	50 °C	55 °C	
G FCC[b]	140.15	133.98	117.97	2.20

FCC, fiber–cement composite without bacterial nanocellulose; fiber–cement composites with bacterial nanocellulose incorporation in powder (P FCC), coated (C FCC), and gel form (G FCC)

[a] Experimental error below 4%

[b] γ_S^D extrapolated to 25 °C = 186 mJ m^{-2}

using the energetic profile of the surface heterogeneity as determined by the BET model (Conder and Young 1979) by injection of different concentrations of *n*-octane. Symmetrical peaks and linear adsorption isotherm, as described by Henry's law, were obtained for all samples under study. As seen in Fig. 1a, production of the FCCs gave rise to more dispersive active sites with higher surface energy (A_{max} of 15 kJ mol^{-1}) compared with the raw materials (A_{max} below 10 kJ mol^{-1}). On incorporation of BNC into the FCC, γ_S^D increased significantly, due to the increased number of active sites with high energy (Fig. 1b). Incorporation of BNC as gel led to a greater increase of 138% in the γ_S^D value (186 mJ m^{-2} when extrapolated to 25 °C) compared with incorporation coated on fibers (48%) or in powder form (10%). The unexpectedly high γ_S^D values found for incorporation of BNC in gel form demonstrate that the surface energy depends not only on the composition of the composite but also on the form of BNC incorporated. The work presented by Benzarti et al. (2006) also showed that the nature, structure, and chemical composition of cement compounds significantly affect their surface dispersion properties.

Energy-dispersive X-ray spectroscopy (EDX) was carried out to provide complementary data and investigate the relationship between the surface composition and surface properties of the materials. The EDX composition results (Table 2) indicated different behavior for the cement, fiber, and BNC in the FCCs produced. The high weight percentage of carbon (C) indicates that the surface of the FCC, P FCC, and G FCC composites was richer in organics/cellulose material.

The high carbon content at the surface together with the higher-energy active sites (Fig. 1b) explain the higher γ_S^D value found for G FCC. In the case of C FCC, the surface shows abundant inorganic material, which may be due to retention of cement particles on the surface of the coated fibers. This indicates that coating the fibers with BNC prevents access by inorganic particles, keeping them at the surface. This protection indicates effective BNC coating of the bagasse fibers. The BNC-coated fibers showed EDX composition similar to the BNC, again confirming that BNC was coated effectively onto the fibers (Fig. 2f). SEM imaging supported this deduction (Fig. 2c, e), where fiber surfaces seemed to be covered with a protective layer of BNC (Accumulation of inorganic materials is indicated by arrows). Moreover, more fibers were pulled out from the cement matrix in C FCC compared with the other composites.

Studying the dependence of γ_S^D on temperature ($\Delta\gamma_S^D/\Delta T$) enables prediction of the structural entropy. The FCCs with added BNC presented stronger temperature dependence (1.31–2.63 mJ m^{-2} K^{-1}) compared with FCC or raw material (0.11–0.44 mJ m^{-2} K^{-1}) (Table 1). As decreased structural

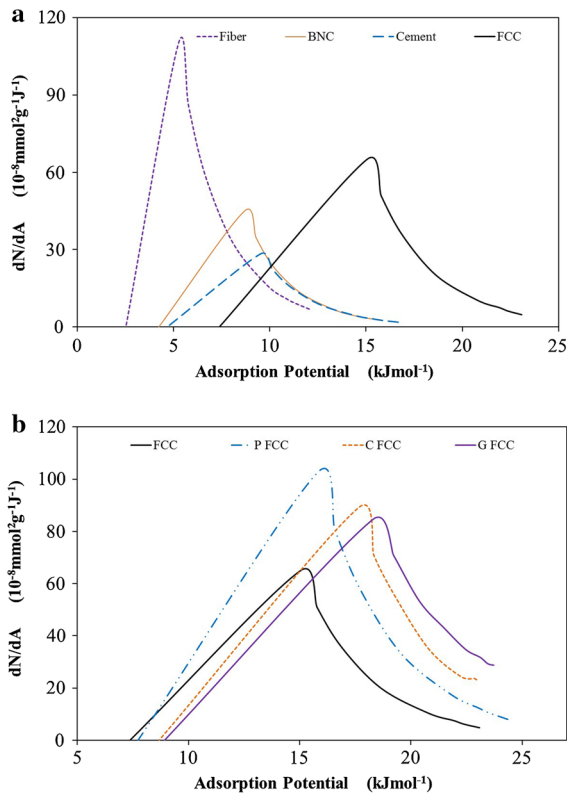

Fig. 1 Energetic profiles obtained using *n*-octane probe for raw materials (**a**) and bagasse fiber–cement composites (**b**). *BNC* bacterial nanocellulose; *FCC* fiber–cement composite without bacterial nanocellulose; fiber–cement composites with bacterial nanocellulose incorporation in powder (P FCC), coated (C FCC), and gel form (G FCC)

organization increases entropic factors, the greater structural organization presented by the raw material was affected by the degree of mixture between the different components, i.e., organics and inorganics. C FCC presented greater structural surface disorganization, as would be predicted based on the fiber protective layer of BNC mentioned above. The EDX results for C FCC showed a higher C/Ca weight ratio in the lumen, indicative of lower mineralization (Table 2), confirming the fiber protection by the BNC mentioned above. On the other hand, FCC presented the lowest entropy, possibly due to greater mineral penetration into the lumen of the fibers.

To relate the surface energy to the surface chemistry of the materials, the $\Delta\gamma_S^D/\Delta T$ values were plotted versus the C/Ca weight ratio, as determined by EDX (Fig. 3a). This weight ratio was chosen as a semi-quantitative measure of the organic versus inorganic material content. We observed an increasing trend of entropy with decreasing calcium content (inorganic materials) loaded in the lumen of the fibers. Thus, less mineralization resulted in stronger temperature dependence of γ_S^D.

It is well known that cement production is a chemical process comprising several reactions, leading to formation of hydrates by reaction of anhydrous cement powder and water. As the variation of the surface energy with humidity can provide important information regarding the effect of FCC hydration on

Table 2 EDX results for elemental composition of raw materials and bagasse fiber–cement composites, at the surface and inside the fiber lumen

Sample	Elemental composition (wt%)				
	C	O	Ca	Si	C/Ca
Bagasse fibers	58.85	38.50	–	–	–
Bacterial nanocellulose	42.36	49.62	–	–	–
Bacterial nanocellulose coated fibers	45.35	53.17			
Portland cement	3.46	8.00	72.29	1.00	0.05
On the surface[a]					
FCC	42.61	17.04	17.30	3.12	2.46
P FCC	48.25	19.21	15.12	4.28	3.19
C FCC	27.76	30.43	20.83	3.61	1.33
G FCC	51.10	26.42	9.18	1.91	5.56
Inside the lumen of fibers[a]					
FCC	45.81	10.88	29.47	2.79	1.55
P FCC	47.50	18.15	24.47	3.06	1.94
C FCC	63.81	12.44	9.66	6.77	6.61
G FCC	53.16	22.88	16.25	1.93	3.27

FCC, fiber–cement composite without bacterial nanocellulose; fiber–cement composites with bacterial nanocellulose incorporation in powder (P FCC), coated (C FCC), and gel form (G FCC)

[a] Mohammadkazemi et al. (2015)

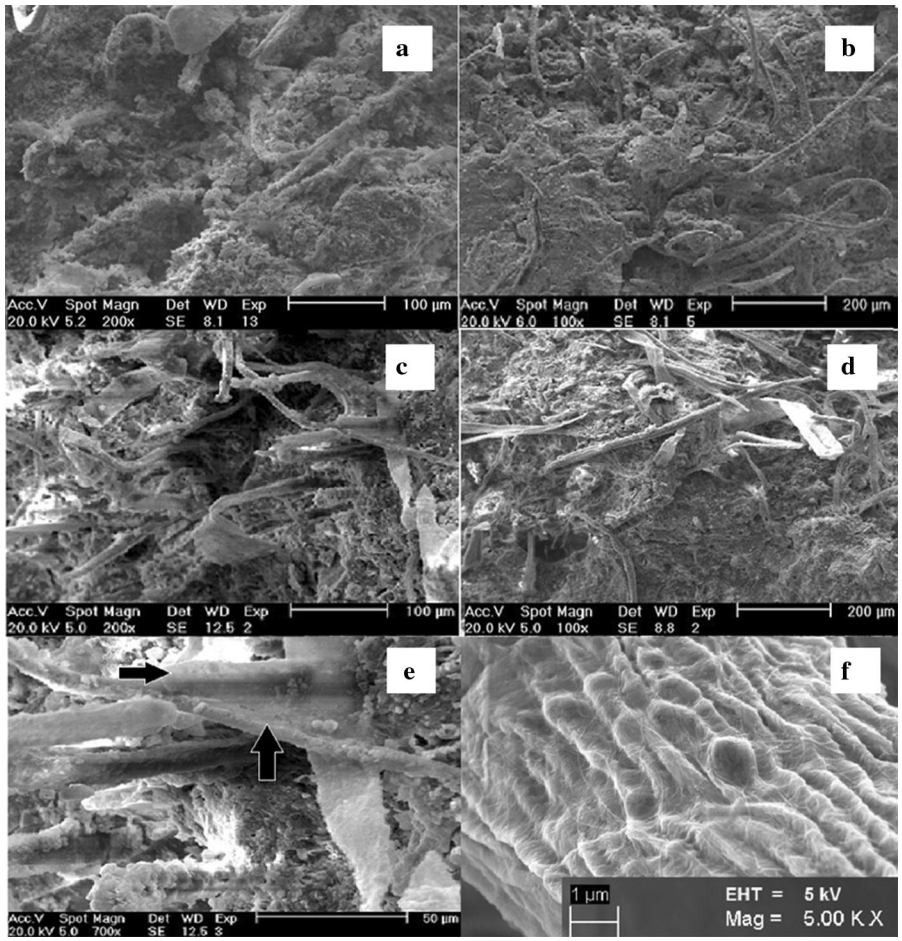

Fig. 2 SEM micrographs of bagasse fiber–cement composites without bacterial nanocellulose (**a**), and with bacterial nanocellulose in powder form (**b**), coated onto the fibers (**c**), in gel form (**d**), and coated onto the fibers at higher magnification (**e**). FE-SEM micrograph of BNC-coated fibers (**f**)

its surface properties, wet (10% RH) carrier gas was used to determine the role of humidity in the adsorption phenomena. The results summarized in Table 3 indicate that the surface energy changed with the hydration, showing a decrease in the γ_S^D values with increasing cement hydration (Fig. 3b). Similar observations were found for illite and kaolinite minerals by Balard et al. (1997) and clay by Cordeiro et al. (2010).

The data in Table 3 also show that different BNC forms (powder, gel, and coated on fiber) induced different water adsorption behavior of the surface.

An interesting correlation was found between the surface energy variation with hydration ($\Delta\gamma_S^D$) and the C/Ca weight ratio on the FCC surface (Fig. 3b): an increase in the C/Ca weight ratio increased the surface energy variation with hydration. So, increasing the organic material at the surface made the surface of the composites more susceptible to humidity. To confirm the susceptibility of the composites to humidity, their water absorption was measured (Table 3). These results revealed that G FCC was more susceptible to hydration, as predicted by IGC. The increased water absorption with BNC incorporation may be due to high BNC swelling, related to its unique structure.

Specific surface energy

To determine the surface acid–base properties, the interactions with five polar molecules were studied. Acetonitrile as an amphoteric probe displayed stronger interaction with the FCCs than the raw materials (Fig. 4), indicating the presence of more energetic

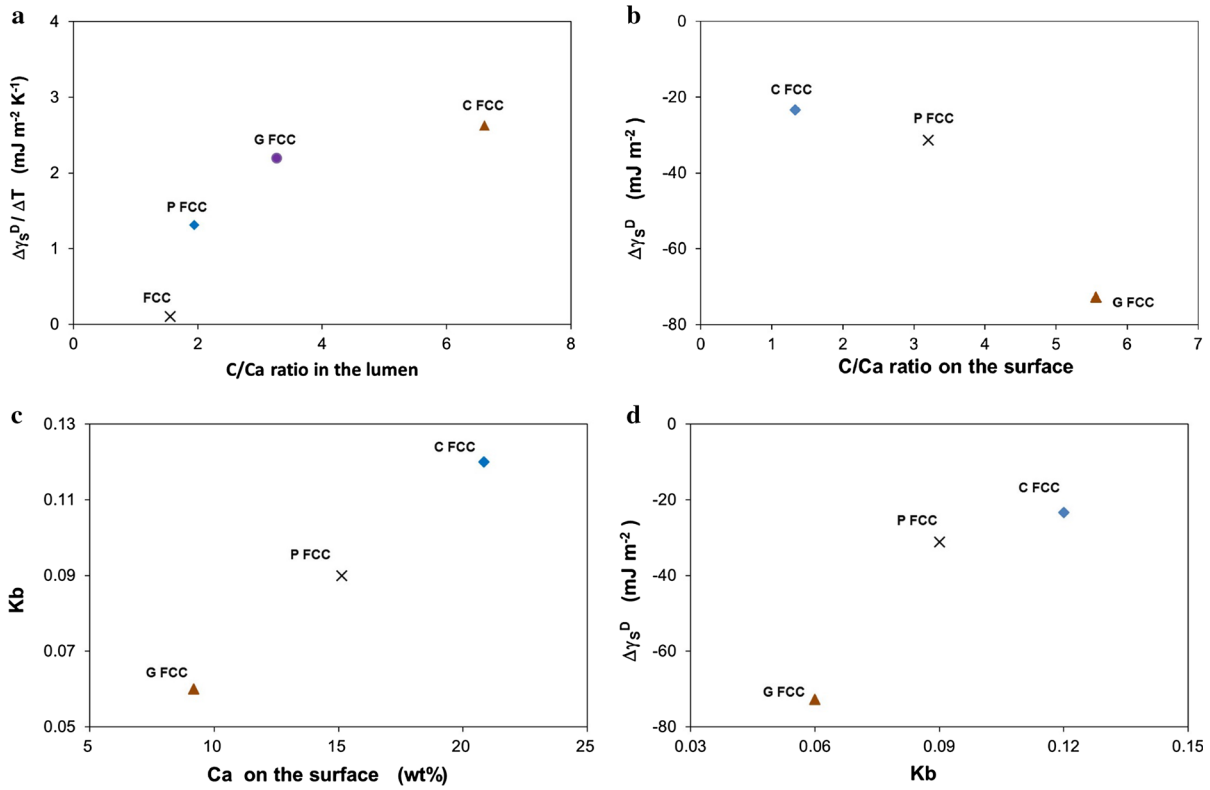

Fig. 3 Relation between EDX weight composition and IGC results: C/Ca ratio in fiber lumen versus $\Delta\gamma_S^D/\Delta T$ (**a**), C/Ca ratio on surface versus $\Delta\gamma_S^D$ (0 and 10% RH) (**b**), Ca amount (wt%) on surface versus K_b (**c**), and K_b versus $\Delta\gamma_S^D$ (0 and 10% RH) (**d**)

Table 3 Variation of dispersive component of surface energy (γ_S^D) with relative humidity and percentage of water absorption (WA, %) in bagasse fiber–cement composites

Sample	γ_S^D (mJ m^{-2})		$\Delta\gamma_S^D$ (%)	WA (%)[a]
	0% RH	10% RH		
FCC	78.15	77.64	−1	13.21
P FCC	86.05	59.26	−31	18.62
C FCC	115.45	88.53	−23	20.46
G FCC	133.98	36.58	−73	26.65

FCC, fiber–cement composite without bacterial nanocellulose; fiber–cement composites with bacterial nanocellulose incorporation in powder (P FCC), coated (C FCC), and gel form (G FCC)

[a] Measured WA during 2 h; RH: relative humidity

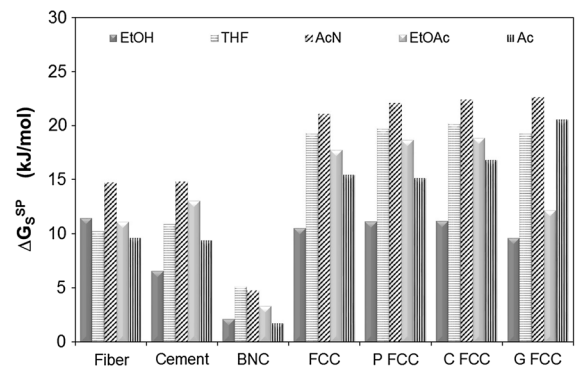

Fig. 4 Specific surface energy (ΔG_S^{sp}) for ethanol (EtOH), tetrahydrofuran (THF), acetonitrile (AcN), ethyl acetate (EtOAc), and acetone (AC) probes for bagasse fibers, Portland cement, and fiber–cement composites without (FCC) and with bacterial nanocellulose in powder (P FCC), coated (C FCC), and gel form (G FCC)

polar active sites on the FCC surface. This means that the FCC surface is more reactive with polar molecules than the Portland cement. With BNC addition to the FCC, slight variation in the acetonitrile ΔG_S^{sp} values was observed.

The ΔG_S^{sp} values measured using the five probes were converted into acid–base constants (K_a and K_b) using Gutmann's (1978) concept. The linear fit ranged from 0.972 to 0.996, meaning that Gutmman's acid

concept is valid for the samples under study and the specific interactions may be considered as being of electron donor–acceptor type. These results showed that the raw materials presented a predominantly basic surface with K_a/K_b ratio of around 0.5 (Table 4). However, the produced FCCs presented a predominantly acid surface with K_a/K_b ratio between 2.00 and 5.75, revealing that FCC production led to great structural surface changes, namely to Portland cement, the major constituent.

The composition of cementitious materials is complex, with several different mineral phases. To obtain more information about the structure and composition of the composites, XRD analysis was performed (Fig. 5).

According to the phase identification, different hydration products such as portlandite [$Ca(OH)_2$], tobermorite ($CaO{\cdot}SiO_2{\cdot}H_2O$), ettringite ($Ca_6[Al(OH)_6]_2(SO_4)_3{\cdot}26H_2O$), larnite ($Ca_2SiO_4$), calcite ($CaCO_3$), and hydrocalumite ($C_3A{\cdot}CaCl_2{\cdot}10H_2O$) were recognized. Among these components, portlandite [calcium hydroxide (CH) with signals at $2\theta = 18°$, 28.68°, 29.2°, 34.08°, 47°, and 54.32°] and tobermorite [calcium silicate hydrate (CSH) with signals at $2\theta = 22.5°$, 24°, 29.2°, 29.5°, 32.2°, 34.5°, 38.5°, 41.3°, 42.7°, 44.5°, 50°, and 53.1°] were the main hydration products. The CH XRD peaks reveal that the CH content on the surface was predominant. The peak at 22.4°, which corresponds to cellulosic components, was higher for the FCCs containing BNC. The peak at 29.2°, attributed to both CSH and calcite, showed the highest intensity in G and C FCC, confirming the predominance of inorganic materials at the surface. In previous work, Perruchot et al. (2006) showed that CSH is characterized by a relatively high γ_S^d value, which can be related to the results for C FCC and G FCC in Table 3.

CSH formation during FCC production is evidenced in the FTIR spectra of the composites through the increase of the O–H stretching vibration band at 3430 cm^{-1} (O–H with hydrogen bond) and the very fine signal at 3640 cm^{-1}, assigned to O–H in the CH structure. In addition, the bending vibration band of molecular H_2O at 1630 cm^{-1} and the asymmetrical stretching vibrations attributed to Si–O bands at around 970 cm^{-1} appeared (Fig. 6). All spectra displayed intense bands attributed to carbonation of various hydrates at 1425 and 870 cm^{-1} (Djouani et al. 2011).

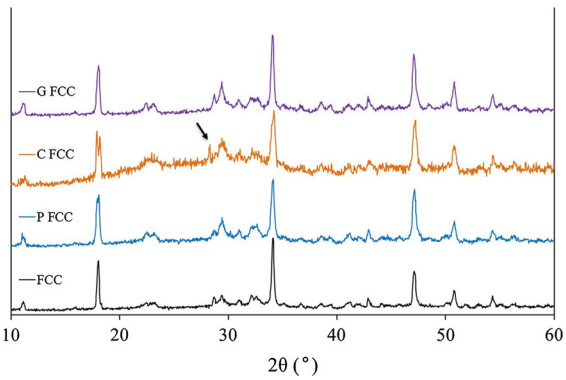

Fig. 5 X-ray diffraction spectra of fiber–cement composites without bacterial nanocellulose (FCC) and with bacterial nanocellulose in powder (P FCC), coated (C FCC), and gel form (G FCC)

Table 4 Acid and base constants (K_a and K_b), BET specific surface area (S_{BET}), and degree of permeability (D_p) of raw materials and bagasse fiber–cement composites

Sample	K_a	K_b	K_a/K_b	S_{BET} ($m^2\ g^{-1}$)	D_p ($cm^2\ seg^{-1}$)
Bagasse fibers	0.12	0.24	0.50	2.06	2.9×10^{-2}
Bacterial nanocellulose	0.06	0.11	0.55	0.23	1.9×10^{-4}
Portland cement	0.13	0.22	0.59	1.59	5.2×10^{-5}
FCC	0.23	0.08	2.88	1.19	1.0×10^{-3}
P FCC	0.23	0.09	2.56	1.05	1.4×10^{-4}
C FCC	0.24	0.12	2.00	2.79	1.1×10^{-5}
G FCC	0.23	0.04	5.75	2.42	6.0×10^{-5}

FCC, fiber–cement composite without bacterial nanocellulose; fiber–cement composites with bacterial nanocellulose incorporation in powder (P FCC), coated (C FCC), and gel form (G FCC)

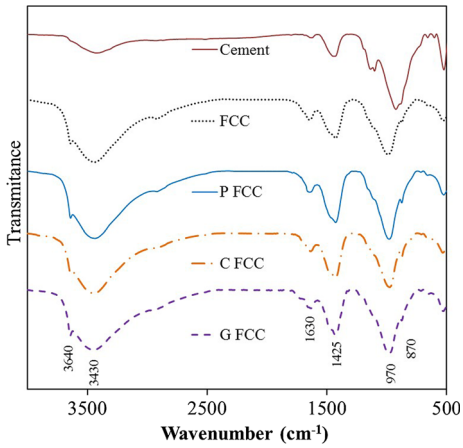

Fig. 6 FTIR spectra of fiber–cement composites without bacterial nanocellulose (FCC) and with bacterial nanocellulose in powder (P FCC), coated (C FCC), and gel form (G FCC)

Since CSH and CH are the main hydration products in hardened cement pastes, it was expected that both acid and basic characteristics would be found for these materials. From the K_a and K_b values (Table 4) and FTIR spectra, it can be inferred that the acid–base variation of the BNC or FCC surface depends particular on the basic sites of the surface (variation of K_b), which differ with the BNC form (powder, coated on fibers, or gel) incorporated into the composite. Again, to relate the surface properties with the surface chemistry of the materials, the calcium content of the fiber surface was correlated with the basic component of the surface energy. Figure 3c presents an excellent linear correlation, showing that the surface basicity of the composites depended on the calcium content at the fiber surface: the higher the calcium content, the higher the affinity of the FCC to acidic molecules.

Since water is a polar molecule, the relationship between the acid–base surface and the hydration effect on the surface energy was studied. Figure 3d proves that the hydration depended on the surface basicity.

Surface area and permeability

IGC isotherm experiments were performed using *n*-octane as probe molecule. The determination of the S_{BET} values showed good correlation coefficients (0.983–0.998), as well as good permeability coefficient values (0.991–0.999) for all the studied materials. These correlations indicate suitability of the IGC technique for the materials under study.

The S_{BET} (Table 4) value was lowest for BNC at 0.23 $m^2\ g^{-1}$, due to its unique compact three-dimensional structure with lower surface roughness, giving rise to lower permeability, compared with bagasse fibers. The other raw materials exhibited greater surface area: the value for bagasse fibers can be explained by nanorugosities and irregularities present on the surface of the fibers (Satyanarayana et al. 2013), which increase the contact area between the fibers and probe. Higher permeability was observed for the fibers due to their low level of material compaction, in contrast to the cement with higher compaction and consequently smaller permeability. Similar values are given in literature for BNC (Castro et al. 2015; Mohammadkazemi et al. 2016), vegetal fiber (Ashori et al. 2013), and cement-like materials (Cordeiro et al. 2010).

From Table 4, it is obvious that BNC addition and also the form of BNC incorporated into the cement clearly influenced the surface area and permeability. Thus, FCC with BNC addition was less permeable, with D_p 10 or 100 times lower, compared with the FCC without BNC. This can be attributed to the lower porosity of BNC/FCCs due to the strong bonding developed by the BNC, giving rise to a packing effect. C and G FCC showed lower D_p values, indicating better interaction/compatibility between the cement and cellulosic material, predicting that these composites will present better mechanical properties. The chemical process and hydration temperature are affected by BNC addition (Mohammadkazemi et al. 2015). The interaction between the constituents of the composites was also revealed by the change of the isotherm. Thus, the raw materials (bagasse fibers, BNC, and cement) presented a type I isotherm, characteristic of adsorption by microporous solids. However, the FCCs presented a type II isotherm, an adsorption mechanism typical of nonporous solids (Gregg and Sing 1982).

Despite the decreased porosity of C and G FCC, increased S_{BET} was observed, predicting an increment in the roughness of the surface of the composite when C and G BNCs were added to the FCC.

Conclusions

The surface properties of bagasse fiber–cement composites and the influence of addition of bacterial nanocellulose were investigated using inverse gas chromatography (IGC). The results demonstrate the

extraordinary ability of the IGC technique to detect surface effects in the production of bagasse fiber–cement composites, and that incorporation of nano-sized bacterial cellulose represents a new green approach to control and/or modify the interaction between fibers and cementitious material.

IGC showed that: (1) the decrease in the mineralization intensified the temperature dependence of the surface energy; (2) by increasing the organic material at the surface, the composites became more susceptible to humidity; (3) the hydration of the composites depended on their surface basicity.

Incorporation of BNC in powder form increased the γ_S^D value by 10% and the basicity slightly, and decreased the fiber mineralization and porosity of the surface of the composite. However, incorporation of BNC coated on fibers increased the γ_S^D value by 48%, while significantly decreasing the fiber mineralization, coupled with a great increase in the surface basicity. On the other hand, incorporation of BNC in gel form increased the γ_S^D value by 138%, increasing the organic components at the surface and greatly decreasing the surface basicity. Lower porosity and greater surface roughness were observed when BNC was used.

According to this study, BNC is highlighted as an attractive green additive (especially when coated onto fibers or in gel form) for production of biocement composites for biological and industrial applications. The improved mechanical properties of the composites, as well as the prevention of fiber mineralization and penetration of alkaline ions, could justify the cost of BNC production. Also, if BNC is produced using cheap culture media, highly productive strains, and simple processes, large-scale production is possible, making use of BNC more economically viable.

Acknowledgments This work was supported by a grant from credit research of Shahid Beheshti University G.C. (contract no. 600/2055). The authors would also like to thank the *Programa Nacional de Re-equipamento Científico*, POCI 2010, for sponsoring IGC work (FEDER and Foundation for Science and Technology). Moreover, the help of Marisa Faria in laboratory work is appreciated.

References

Ashori A, Cordeiro N, Faria M, Hamzeh Y (2013) Effect of chitosan and cationic starch on the surface chemistry properties of bagasse paper. Int J Biol Macromol 58:343–348

Baeta Neves MI, Oliva V, Mrabet B, Connan C, Chehimi MM, Delamar M, Hutton S, Roberts A, Benzarti K (2002) Surface chemistry of cement pastes: a study by X-ray photoelectron spectroscopy. Surf Interface Anal 33:834–841

Baeta Neves I, Chabut M, Perruchot C, Chehimi MM, Benzarti K (2004) Interfacial interactions of structural adhesive components with cement pastes: studies by inverse gas chromatography (IGC). Appl Surf Sci 238:523–529

Balard H, Saada A, Siffert B, Papirer E (1997) Influence of water on the retention of organic probes on clays studied by IGC. Clay Clay Miner 45:489–495

Benzarti K, Perruchot C, Chehimi MM (2006) Surface energetics of cementitious materials and their wettability by an epoxy adhesive. Colloid Surf A 286:78–91

Boukerma K, Piquemal J-Y, Chehimi MM, Mravčáková M, Omastová M, Beaunier P (2006) Synthesis and interfacial properties of montmorillonite/polypyrrole nanocomposites. Polymer 47:569–576

Boutboul A, Lenfant F, Giampaoli P, Feigenbaum A, Ducruet V (2002) Use of inverse gas chromatography to determine thermodynamic parameters of aroma–starch interactions. J Chromatogr A 969:9–16

Carmona-Quiroga PM, Rubio J, Sánchez MJ, Martínez-Ramírez S, Blanco-Varela MT (2011) Surface dispersive energy determined with IGC-ID in anti-graffiti-coated building materials. Prog Org Coat 71:207–212

Castro C, Cordeiro N, Faria M, Zuluaga R, Putaux J-L, Filpponen I, Velez L, Rojas OJ, Gañán P (2015) In-situ glyoxalization during biosynthesis of bacterial cellulose. Carbohydr Polym 126:32–39

Conder J, Young C (1979) Physicochemical measurements by gas chromatography. Wiley, NY

Cook RA, Hover KC (1993) Mercury porosimetry of cement-based materials and associated correction factors. Constr Build Mater 7:231–240

Cordeiro N, Silva J, Gomes C, Rocha F (2010) Bentonite from Porto Santo Island, Madeira archipelago: surface properties studied by inverse gas chromatography. Clay Miner 45:77–86

Cordeiro N, Gouveia C, John MJ (2011a) Investigation of surface properties of physico-chemically modified natural fibres using inverse gas chromatography. Ind Crop Prod 33:108–115

Cordeiro N, Gouveia C, Moraes AGO, Amico SC (2011b) Natural fibers characterization by inverse gas chromatography. Carbohydr Polym 84:110–117

Cordeiro N, Ornelas M, Ashori A, Sheshmani S, Norouzi H (2012) Investigation on the surface properties of chemically modified natural fibers using inverse gas chromatography. Carbohydr Polym 87:2367–2375

Courard L (1999) How to analyze thermodynamic properties of solids and liquids in relation with adhesion? In: Ohama Y, Puterman M (eds) ISAP 99, proceedings of the 2nd international RILEM symposium on adhesion between polymers and concrete, Dresden

Djouani F, Connan C, Delamar M, Chehimi MM, Benzarti K (2011) Cement paste–epoxy adhesive interactions. Constr Build Mater 25:411–423

Elizalde-González MP, Ruíz-Palma R (1999) Gas chromatographic characterization of the adsorption properties of the

natural adsorbent CACMM2. J Chromatogr A 845: 373–379

Fan MZ, Bonfield PW, Dinwoodie JM, Breese MC (1999) Dimensional instability of cement-bonded particleboard: mechanisms of deformation of CBPB. Cem Concr Res 29:923–932

Fan MZ, Bonfield PW, Dinwoodie JM, Boxall J, Breese MC (2004) Dimensional instability of cement-bonded particleboard: the effect of surface coating. Cement Concr Res 34:1189–1197

Grattoni CA, Chiotis ED, Dawe RA (1995) Determination of relative wettability of porous sandstones by imbibition studies. J Chem Technol Biotechnol 64:17–24

Gregg SJ, Sing KSW (1982) Adsorption, surface area and porosity. Academic, San Diego

Gulati D, Sain M (2006) Surface characteristics of untreated and modified hemp fibers. Polym Eng Sci 46:269–273

Gutmann V (1978) The donor–acceptor approach to molecular interactions. Plenum, New York

John VM, Agopyan V, Prado TA (1998) Durability of cement composites and vegetable fibers for roofing. In: Proceedings of 3rd Ibero-American symposium on Roofing for Housing. Cyted/USP, São Paulo pp 51–59

Keller UJ, Staudt R (2005) Gas adsorption equilibria: experimental methods and adsorption isotherms. Springer, New York

Milczewska K, Voelkel A (2002) Characterization of the interactions in polymer–filler systems by inverse gas chromatography. J Chromatogr A 969:255–259

Mohammadkazemi F, Doosthoseini K, Ganjian E, Azin M (2015) Manufacturing of bacterial nano-cellulose reinforced fiber–cement composites. Constr Build Mater 101(Part 1):958–964

Mohammadkazemi F, Faria M, Cordeiro N (2016) In situ biosynthesis of bacterial nanocellulose-$CaCO_3$ hybrid bionanocomposite: one-step process. Mater Sci Eng C 65:393–399

Momber AW (2002) The wettability of some concrete powders. Part Sci Technol 20:243–246

Morton JH, Cooke T, Akers SAS (2010) Performance of slash pine fibers in fiber cement products. Constr Build Mater 24:165–170

Neithalath N, Weiss J, Olek J (2004) Acoustic performance and damping behavior of cellulose–cement composites. Cem Concr Comp 26:359–370

Oliva V, Mrabet B, Baeta Neves MI, Chehimi MM, Benzarti K (2002) Characterisation of cement pastes by inverse gas chromatography. J Chromatogr A 969:261–272

Papirer E, Brendle E, Ozil F, Balard H (1999) Comparison of the surface properties of graphite, carbon black and fullerene samples, measured by inverse gas chromatography. Carbon 37:1265–1274

Perruchot C, Chehimi MM, Vaulay M-J, Benzarti K (2006) Characterisation of the surface thermodynamic properties of cement components by inverse gas chromatography at infinite dilution. Cem Concr Res 36:305–319

Philippi PC, Souza HA (1995) Modelling moisture distribution and isothermal transfer in a heterogeneous porous material. Int J Multiph Flow 21:667–691

Satyanarayana PVV, Rao KP, Kumar UA, Sivaramakrishna K (2013) Bulk utilization of fly ash lime sodium silicate mixes in geotechnical applications. Pollut Res Paper 32:353–356

Savastano H Jr, Warden PG, Coutts RSP (2003) Mechanically pulped sisal as reinforcement in cementitious matrices. Cem Concr Comp 25:311–319

Tolêdo Filho RD, Ghavami K, England GL, Scrivener K (2003) Development of vegetable fibre–mortar composites of improved durability. Cem Concr Comp 25:185–196